JURNAL KARTIKA KIMIA

J. Kartika Kimia, November 2025, 8, (2), 230-243
Journal homepage: http://jkk.unjani.ac.id/index.php/jkk
P-ISSN: 2655-1322 E-ISSN: 2655-0938

Molecular Docking and ADMET Analysis of Flavonoid Compounds from Bajakah Tampala Stem (Spatholobus littoralis Hassk.) Targeting VEGFR-2 and c-MET

Dzava Prawinsyah Fairus Ismail[1,*], Nafis Shafa[1], Violent Irene Pendy[1], George Patrick Devon[1], Yenny Febriani Yun[2]
[1]Bachelor Program in Pharmacy, Faculty of Pharmacy, Universitas Padjadjaran, Sumedang 45363, Indonesia
[2]Department of Chemistry, Faculty of Science and Informatics, Universitas Jenderal Achmad Yani, Cimahi 40531, Indonesia
*E-mail: dzava22001@mail.unpad.ac.id

DOI: https://doi.org/10.26874/jkk.v8i2.982

Received: 25 Aug 2025, *Revised*: 28 Feb 2026, *Accepted*: 3 March 2026, *Online*: 19 March 2026

Abstract

Cancer is a condition marked by abnormal and uncontrolled cell growth, with VEGFR-2 and c-MET receptors contributing to tumor angiogenesis, metastasis, and resistance to therapy. Bajakah tampala stem (*Spatholobus littoralis* Hassk.) is a traditional plant from Kalimantan that is rich in flavonoid compounds that may interact with these molecular targets. This study aimed to evaluate the molecular interactions, drug-likeness, and pharmacokinetic properties of Bajakah flavonoid compounds through in silico approaches. Lipinski's rule of five and ADMET predictions indicated favorable drug-likeness and absorption profiles for most compounds, although some displayed moderate intestinal absorption and potential mutagenicity. Among the evaluated compounds, hesperetin showed the most favorable predicted binding affinity toward VEGFR-2 (binding energy -9.57 kcal/mol; predicted Ki 97.00 nM), while apigetrin demonstrated the lowest predicted binding energy toward c-MET (-9.43 kcal/mol; predicted Ki 122.94 nM). Both compounds exhibit interactions comparable to reference drugs cabozantinib and crizotinib, suggesting their potential as natural lead compounds for anticancer therapy. Further in vitro and in vivo studies are warranted to confirm their efficacy and safety.

Keywords: Bajakah, Flavonoid, In silico, Molecular docking, *Spatholobus littoralis*

1 Introduction

Cancer is a group of diseases that is characterized by uncontrolled cellular proliferation that could infiltrate adjacent tissues and cells [1] . In 2022, the World Health Organization's Global Cancer Observatory estimated approximately 9.7 million cancer deaths worldwide. The leading cause of death from the most commonly diagnosed types of cancer is lung cancer, with an estimated 20 million new cases diagnosed in the same year, followed by breast cancer in women and colorectal cancer [2] .

One of the receptors involved in cancer is VEGFR-2, which stimulates the formation of new blood vessels to help tumors by bringing nutrients and oxygen for them to grow. Another receptor that helps cancer cells survive, multiply, and spread is c-MET. Together, they all work to worsen cancer progression by fueling angiogenesis, spreading the disease, and even helping tumors resist treatment [3,4]. When a pathway is blocked, tumors frequently turn to the other as a fallback, making cancer harder to treat. Therefore, targeting both VEGFR-2 and c-MET simultaneously is a promising method of blocking the tumor's growth and survival. Drugs that block both receptors, such as cabozantinib and crizotinib, have shown anticancer effects and are currently advancing as potential cancer therapies [5].

Cabozantinib is a multitarget kinase inhibitor that effectively inhibits tumor growth and angiogenesis by blocking VEGFR-2 and other pathways such as AXL, RET, and KIT [6]. Similarly, crizotinib is a multi-kinase inhibitor that can suppress tumor growth and angiogenesis

by blocking ALK, ROS1, and c-Met, while also overcoming chemotherapy resistance through JAK2 and mutant Bcr/Abl inhibition [7]. Despite their therapeutic benefits, these drugs are still limited in terms of safety and the development of drug resistance. Some limitations include the emergence of secondary mutations in the receptor target, activation of alternative signaling pathways, and toxic side effects such as hypertension, gastrointestinal disorders, hand-foot syndrome, and fatigue. These shortcomings can reduce long-term effectiveness and decrease patient compliance [3]. As a result, there is a need for the development of safer alternative therapies, such as the utilization of natural compounds from plants.

Bajakah tampala stem (*Spatholobus littoralis* Hassk.) is a traditional plant from Kalimantan that has gained attention as a natural alternative for cancer therapy because it contains abundant flavonoids that are linked to strong biological activities [8]. Furthermore, the ethyl acetate fraction of bajakah tampala extract has been shown to exert anticancer effects through their reported IC_{50} value of 4.79 µg/mL against the T47D breast cancer cell line [9]. This suggests that bajakah tampala demonstrates high cytotoxic activity towards cancer cells, and therefore the flavonoid compounds contained in the bajakah tampala stem are a promising natural candidate for further development in the cancer treatment [10]. Even though their potential as anticancer agents was discovered through in vitro studies, their molecular mechanisms remained unknown. Therefore, this study aims to identify the molecular interactions of *S. littoralis* Hassk. flavonoid compounds towards VEGFR-2 and c-MET as anticancer through molecular docking, as well as their drug-likeness and ADMET properties.

2 Method

2.1. Materials and tools

In silico analyses were conducted on a personal laptop with an AMD Ryzen 3 3250U processor with Radeon Graphics 2.60 GHz, 8.00 GB RAM, and Windows 64-bit operating system. The protein targets examined in this study included the VEGFR-2 receptor (PDB ID: 2P2I) and c-MET receptor (PDB ID: 3ZZE) along with their native ligands which are obtained from Protein Data Bank of RCSB (https://www.rcsb.org) and then prepared in BIOVIA Discovery Studio 2025 by removing water molecule. Test flavonoid compounds sourced from a previous study and obtained from PubChem were refined through MM2 geometry optimization in Chem3D Pro 12.0, as shown in **Fig. 1** [11]. Additionally, this study employed a range of software and webtools, including BIOVIA Discovery Studio 2025, PubChem, Protein Data Bank, mcule property calculator, Chem3D Pro 12.0, AutoDock 4.2.6, and PreADMET.

2.2. Lipinski's rule of 5 predictions

Lipinski's rule of 5 evaluation was performed by retrieving the SMILES format of each flavonoid compound from PubChem (https://pubchem.ncbi.nlm.nih.gov/) and generating their two-dimensional structure. Each compound is then analyzed using a mcule property calculator (https://mcule.com/apps/property-calculator/) to predict the drug-likeness properties. The parameters assessed for the drug-likeness included molecular weight, log P, hydrogen bond donor, and acceptor.

2.3. ADMET predictions

ADMET predictions were conducted by obtaining the flavonoid compounds and analyzing them through PreADMET (https://preadmet.webservice.bmdrc.org/). The pharmacokinetic parameters assessed were human intestinal absorption (HIA), blood-brain barrier (BBB) penetration, plasma protein binding (PPB), and Caco-2 cell permeability. In addition, toxicity parameters such as carcinogenicity to rodent and Ames test mutagenicity were also evaluated.

2.4. Molecular docking simulation

Ligand geometry optimization was carried out before molecular docking by using molecular mechanics (MM2) calculations in Chem3D Pro 12.0. Each ligand was constructed and subjected to energy minimization to minimum RMS gradient of 0.010 using MM2 calculations.

Molecular docking protocol validation was performed by re-docking each native ligands into their respective receptors using Autodock 4.2.6. The grid box dimensions and coordinates were adjusted to yield RMSD ≤ 2 Å and a negative binding energy, with a Lamarckian Genetic Algorithm (GA) runs of 100. The grid box parameters for molecular docking were configured as follows: for the VEGFR-2 receptor (PDB ID: 2P2I), the grid box dimensions were set to 40 × 48 × 40 with center coordinates at x = 38.192, y = 35.014, z = 12.178 and for the c-MET receptor (PDB ID: 3ZZE), the grid box was also

40 × 40 × 40 with center coordinates at x = 17.376, y = 10.965, z = 4.832.

Subsequently, molecular docking simulations were performed between the flavonoid test ligands and the prepared receptors, using cabozantinib (VEGFR-2) and crizotinib (c-MET) as reference drugs. Receptor preparation was conducted in BIOVIA Discovery Studio 2025, which involved the removal of water molecules and separation of the native ligand. Polar regions of the proteins were refined by adding Kollman charges and hydrogen atoms. Ligand preparation in AutoDock 4.2.6 included merging nonpolar hydrogens, adding hydrogen atoms, and assignment of Gasteiger charges. Molecular docking simulations were executed using the Lamarckian Genetic Algorithm with 100 runs, following the same parameters as validation. Binding energy and inhibition constants were obtained through AutoDock, while ligand-receptor interactions were visualized using BIOVIA Discovery Studio 2025.

The best pose in a molecular docking study is generally selected based primarily on the lowest binding energy, high cluster population, low RMSD, and a small inhibition constant value supported by favorable interaction profiles such as hydrogen bonds.

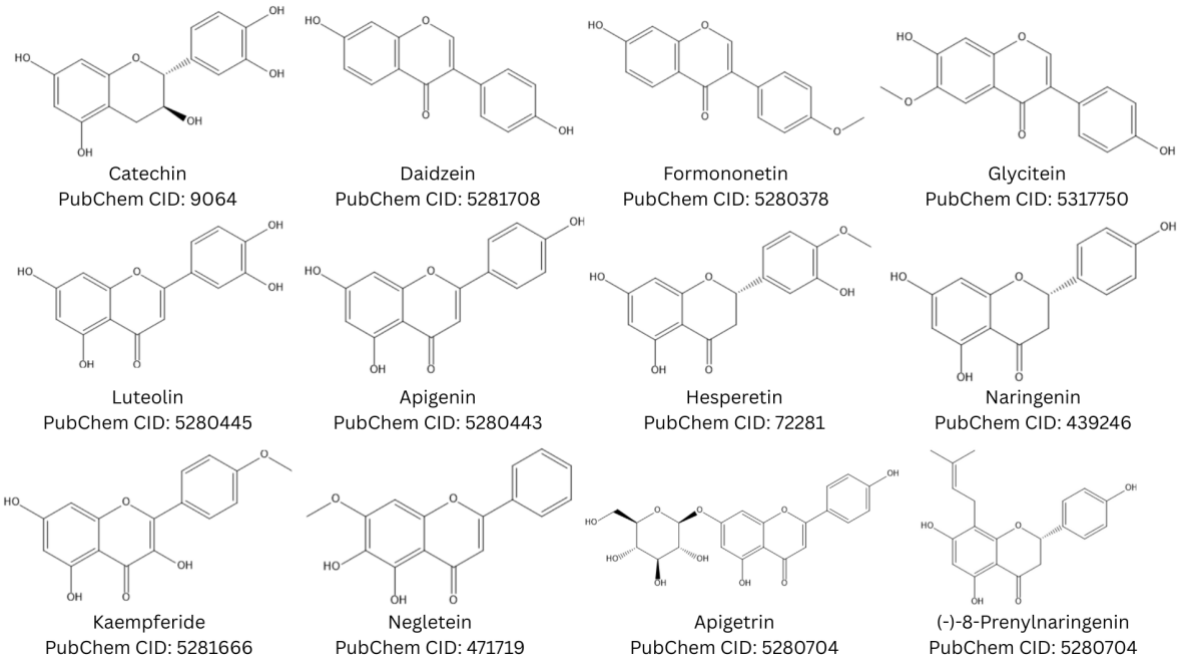

Figure 1. Chemical structure of flavonoids in *S. littoralis* Hassk. used as test ligands.

3 Result and Discussion

3.1. Lipinski's rule of 5 predictions

Lipinski's rule of 5 predictions serves as a guideline to evaluate the drug-likeness and to identify if a compound with pharmacological activity exhibited physicochemical properties that would make it likely orally active drug in humans [12]. According to Lipinski's rule of 5, drug-likeness properties depend on four physicochemical parameters: molecular weight ≤ 500 Da, hydrogen bond donor ≤ 5, hydrogen bond acceptor ≤ 10, and log P ≤ 5 [13]. This rule suggests that an orally active drug should have no more than one violation of the mentioned criteria [14]. These parameters are closely related to intestinal permeability and aqueous solubility, thereby influencing the first step of oral bioavailability in humans. Based on **Table 1**, Lipinski's rule of 5 analysis of tested flavonoid compounds fulfilled the established criteria with the maximum violation of one. Therefore, these findings suggest that these compounds exhibited favorable physicochemical properties and oral bioavailability.

Table 1. Lipinski's rule of 5 predictions results from S. *littoralis* Hassk. flavonoid compounds

Compounds	Molecular weight (Da)	Log P	Hydrogen bond donor	Hydrogen bond acceptor	Lipinski violations
Catechin	290.267	1.546	5	6	0
Daidzein	254.236	2.871	2	4	0
Formononetin	268.263	3.174	1	4	0
Glycitein	284.262	2.880	2	5	0
Luteolin	286.235	2.282	4	6	0
Apigenin	270.236	2.577	3	5	0
Hesperetin	302.278	2.519	3	6	0
Naringenin	272.252	2.510	3	5	0
Kaempferide	300.262	2.585	3	6	0
Negletein	284.262	2.880	2	5	0
Apigetrin	432.376	0.050	6	10	1
(-)-8-Prenylnaringenin	340.369	4.019	3	5	0

3.2. ADMET predictions

ADMET prediction analysis was performed to evaluate the pharmacokinetic behavior and potential toxicity of the flavonoid compounds. Pharmacokinetic parameters such as absorption, distribution, metabolism, and excretion (ADME) were assessed to determine their suitability for systemic administration and utilization [15]. Furthermore, toxicity predictions were carried out to identify the potential risks from the compound that might affect human health [16]. The ADMET prediction results are demonstrated in Table 2.

HIA is a degree that estimates how much a compound is absorbed in the human intestine. Generally, HIA is directly proportional to the intestinal absorption. Therefore, a higher HIA value indicates better intestinal absorption of the compound [17]. The HIA results revealed the flavonoid compounds of *S. littoralis* Hassk. mostly exhibited high HIA values ranging from 79.427% - 95.552%, except catechin and apigetrin which are considered moderate with HIA values of 66.708% and 47.106%, respectively. In order to enhance their intestinal absorption, these compounds could be formulated into a more advanced drug delivery system such as nano emulsions, nanoparticles, or liposomes, which have been widely used to improve the solubility and bioavailability of flavonoids [18–20].

Caco-2 permeability is a model used to identify the passive diffusion of compounds across intestinal epithelium [21]. According to the Caco-2 predictions results, catechin and negletein exhibited low permeability towards Caco-2 with the values of 0.657 nm/sec and 2.767 nm/sec respectively. In contrast, ten other flavonoid compounds possessed moderate Caco-2 permeability, with the values varying from 4.540 nm/sec - 13.033 nm/sec.

PPB is a parameter that indicates how strongly a compound attaches to plasma protein. In general, PPB influences a compound's distribution, free fraction concentration, and pharmacological activity [22]. All flavonoid compounds except apigetrin demonstrated high PPB values (83.992%-100.000%). Apigetrin shows a relatively lower PPB value of 73.433% which indicates a higher proportion of the compound remains in its free fraction inside the circulation. As a result, this greater free fraction may enhance its immediate therapeutic potential [23].

BBB represents a microvascular unit that selectively regulates the permeability of a compound to the brain [24]. Based on the ADMET predictions, formononetin, glycitein, and apigetrin has low BBB penetration with values of 0.063, 0.091, and 0.037 respectively. These findings indicate that these compounds are predicted to exert minimal central nervous system side effects [25]. On the other hand, the rest of the flavonoid compounds exhibited moderate BBB penetration with values extending from 0.117 - 1.934.

One of the most critical observations in the toxicity profile is that all twelve flavonoid compounds were identified as mutagen through the Ames test. For flavonoids, this predicted mutagenicity can be attributed to their characteristic chemical structure. In flavones and flavonols, the presence of a double bond between C2 and C3 in the heterocyclic ring ensures that the entire chromophore maintains a rigid, planar

geometry. This planarity is fundamental for DNA intercalation. When a flavonoid intercalates, it is stabilized by π-π stacking interactions with the nitrogenous bases. This physical insertion can cause unwinding of the DNA helix, leading to mutations during DNA replication [26,27].

Lastly, the carcinogenicity results suggest that although the majority of flavonoids tested were non-carcinogenic in mice and rats, some compounds including luteolin, apigenin, and negletein exhibited positive responses in one or both animal models. Consequently, this raises the need for further efficacy and safety studies towards *S. littoralis* Hassk. flavonoid compounds before their therapeutic utilization as some compounds were predicted to be able to induce genetic mutation or cancer.

Table 2. ADMET predictions results of *S. littoralis* Hassk. flavonoid compound

Compounds	HIA (%)	Caco-2 (nm/sec)	PPB (%)	BBB	Mutagen	Carcinogen	
						Mouse	Rat
Catechin	66.706	0.657	100.000	0.395	Mutagen	-	-
Daidzein	92.646	7.720	88.705	0.194	Mutagen	-	+
Formononetin	95.552	7.601	85.087	0.063	Mutagen	-	+
Glycitein	93.042	7.065	89.437	0.091	Mutagen	-	+
Luteolin	79.427	4.540	99.717	0.368	Mutagen	+	+
Apigenin	88.123	10.547	97.253	0.565	Mutagen	+	+
Hesperetin	87.193	7.004	96.763	0.223	Mutagen	-	+
Naringenin	87.193	10.521	100.000	0.597	Mutagen	-	-
Kaempferide	88.192	9.335	83.992	0.157	Mutagen	-	+
Negletein	93.033	2.767	91.176	0.117	Mutagen	-	+
Apigetrin	47.106	7.217	73.433	0.037	Mutagen	+	-
(-)-8-Prenylnaringenin	90.291	13.033	100.000	1.934	Mutagen	-	-

3.3. Molecular docking simulations

Validation of the molecular docking protocol was performed prior to the simulation in order to identify the active site location of the protein by grid box parameter, which allows the docking simulations to be performed on the respective region of the protein [28]. Generally, RMSD values below 2.0 Å indicate that the docking protocol is capable of predicting the binding orientation of native ligands accurately [29]. The validation of molecular docking protocol results, as shown in Fig 2, demonstrates that the RMSD obtained was 0.63 Å for the native ligand of VEGFR-2 receptor (PDB ID: 2P2I) and 0.93 Å for the native ligand of c-MET receptor (PDB ID: 3ZZE). Therefore, the docking protocol used for this study was deemed as valid.

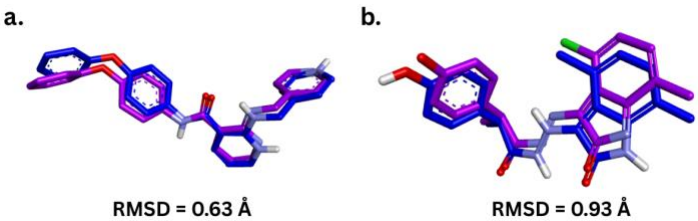

Figure 2. Overlay visualization of native ligands in molecular docking validation (a) VEGFR-2 (PDB ID: 2P2I) (b) c-MET (PDB ID: 3ZZE)

Molecular docking simulations of flavonoid compounds of *S. littoralis* Hassk. were performed on the VEGFR-2 receptor (PDB ID: 2P2I) and c-MET receptor (PDB ID: 3ZZE). The results of molecular docking of each compound towards VEGFR-2 receptor (PDB ID: 2P2I) as

shown in **Table 3** revealed that the most frequently interacting amino acid residues were ASP 1046[a], GLU 885[a], CYS 919[a], PHE 1047[a], and VAL 916[a]. In addition, MET 1160[a], ASP 1222[a], TYR 1230[a], ASN 1209[a], and LEU 1140[a] were also identified as the most frequently interacting amino acid residues in the c-MET (PDB ID: 3ZZE) molecular docking result, as shown in **Table 4**.

Table 3. Molecular docking results of *S. littoralis* Hassk. flavonoid compound against VEGFR-2 receptor (PDB ID: 2P2I)

Compound	Binding Energy (kcal/mol)	Inhibition Constant (Ki)	Interactions with Amino Acid Residue		
			Hydrogen bond	Van der Waals	Other bond
Native Ligand	-11.78	2.3 nM	**Conventional Hydrogen Bond** ASP 1046[a], GLU 885[a] **Carbon Hydrogen Bond** GLU 917[a], ALA 866[a]	PHE 918[a], VAL 898[a], ILE 1044[a], HIS 1026[a], ILE 888[a], ILE 892[a], LYS 868[a], VAL 914[a], VAL 867[a], VAL 848[a], VAL 916[a], PHE 1047[a]	**Pi-Sigma** LEU 1019[a] **Pi-Alkyl** LEU 1035[a], LEU 840[a], VAL 899[a], CYS 1024[a], LEU 889[a] **Unfavorable Donor-Donor** CYS 919[a]
Cabozantinib (reference drug)	-11.10	7.34 nM	**Conventional Hydrogen Bond** ASP 1046[a] **Carbon Hydrogen Bond** ILE 1025[a], HIS 1026[a], GLU 885[a]	GLY 922[a], CYS 1045[a] PHE 1047[a],	**Halogen (Fluorine)** CYS 919[a] **Pi- Anion** GLU 885[a] **Pi-Sigma** LEU 1035[a], LEU 840[a] **Pi-Pi Stacked** PHE 918[a] **Alkyl, Pi-Alkyl** ILE 888[a], LEU 889[a], ALA 1050[a], LEU 1019[a], VAL 898[a], ILE 1044[a], LYS 868[a], VAL 848[a], ALA 866[a]
Catechin	-8.04	1280 nM	**Conventional Hydrogen Bond** CYS 1045[a], GLU 885[a], VAL 914[a], CYS 919[a]	LEU 889[a], ASP 1046[a], PHE 1047[a], GLY 922[a], VAL 867[a], ILE 915[a]	**Pi-Sigma** VAL 916[a], LEU 840[a] **Pi-Pi Stacked** PHE 919[a] **Alkyl, Pi-Alkyl** LYS 868[a], VAL 848[a], LEU 1035[a], ALA 866[a], CYS 1045[a]
Daidzein	-8.06	1230 nM	**Conventional Hydrogen Bond** CYS 919[a], GLU 885[a]	PHE 1047[a], VAL 899[a], CYS 1045[a], LEU 889[a], VAL 914[a], GLU 917[a], LYS 920[a]	**Pi-Sigma** LEU 1035[a], LEU 840[a] VAL 916[a] **Pi-Pi Stacked** PHE 918[a] **Pi-Alkyl**

					ALA 866[a], VAL 848[a], LYS 868[a], CYS 919[a], LEU 1035[a] **Unfavorable Donor-Donor** GLY 922[a]
Formononetin	-7.64	2520 nM	**Conventional Hydrogen Bond** LYS 868[a], GLU 885[a] **Carbon Hydrogen Bond** CYS 919[a]	LEU 889[a], CYS 919[a], GLY 922[a], PHE 918[a], PHE 1047[a], ASP 1046[a]	**Pi-Alkyl** VAL 916[a], VAL 899[a], CYS 1045[a], ALA 866[a], LEU 840[a], LEU 1035[a], VAL 848[a]
Glycitein	-7.76	2050 nM	**Conventional Hydrogen Bond** GLU 885[a], CYS 919[a] **Pi-Donor Hydrogen Bond** ASP 1046[a]	GLU 917[a], PHE 918[a], GLY 922[a], LEU 889[a], LYS 869[a], VAL 848[a]	**Pi-Sigma** LEU 1035[a], LEU 840[a] **Alkyl, Pi-Alkyl** VAL 916[a], VAL 899[a], CYS 1045[a], CYS 919[a], PHE 1047[a], ALA 866[a], LEU 840[a]
Luteolin	-8.96	269.13 nM	**Conventional Hydrogen Bond** VAL 914[a], ALA 866[a], ASP 1046[a], CYS 919[a]	ILE 915[a], VAL 867[a], GLU 885[a], VAL 889[a], PHE 1047[a], GLY 922[a], LYS 920[a]	**Pi-Sigma** VAL 916[a], LEU 1035[a], LEU 840[a] **Pi-Sulfur** CYS 1045[a] **Pi-Pi Stacked** PHE 918[a] **Pi-Alkyl** LYS 868[a], VAL 848[a], VAL 916[a], ALA 866[a]
Apigenin	-9.18	185.86 nM	**Conventional Hydrogen Bond** VAL 914[a], ASP 1046[a], ALA 866[a], CYS 919[a]	ILE 915[a], VAL 867[a], VAL 899[a], GLU 885[a], GLY 922[a], PHE 1047[a]	**Pi-Sigma** VAL 916[a], LEU 1035[a], LEU 840[a] **Pi-Sulfur** CYS 1045[a] **Pi-Pi Stacked** PHE 918[a] **Pi-Alkyl** LYS 868[a], VAL 848[a]
Hesperetin	-9.57	97.00 nM	**Conventional Hydrogen Bond** VAL 914[a], GLU 885[a], ASP 1046[a], CYS 919[a]	LE 915[a], VAL 867[a], VAL 899[a], LEU 889[a], CYS 1045[a], GLY 922[a], PHE 918[a]	**Pi-Cation** LYS 868[a] **Pi-Sigma** VAL 916[a], LEU 1035[a], LEU 840[a] **Pi-Alkyl** VAL 848[a], ALA 866[a], PHE 1047[a]
Naringenin	-9.17	190.68 nM	**Conventional Hydrogen Bond**	LE 915[a], VAL 867[a], VAL 899[a], CYS	**Pi-Sigma**

			ALA 866[a], CYS 919[a]	1045[a], GLY 922[a], PHE 918[a], PHE 1047[a], GLU 885[a]	VAL 916[a], LEU 1035[a] **Pi-Alkyl** VAL 848[a], LEU 840[a]
Kaempferide	-8.83	336.03 nM	**Conventional Hydrogen Bond** GLU 885[a], ASP 1046[a]	ILE 1044[a], VAL 914[a], VAL 898[a], LEU 1035[a]	**Pi-Cation** LYS 868[a] **Pi-Sulfur** CYS 1045[a] **Pi-Pi T-Shaped** PHE 1047[a] **Pi-Alkyl** HIS 1026[a], LEU 889[a], LEU 1019[a], VAL 889[a], VAL 916[a], VAL 848[a], ALA 866[a]
Negletein	-8.25	900.65 nM	**Conventional Hydrogen Bond** GLU 885[a], ASP 1046[a], LYS 868[a]	ILE 915[a], VAL 867[a], CYS 1045[a], GLY 922[a]	**Pi-Sigma** PHE 1047[a], VAL 916[a] **Pi-Alkyl** CYS 919[a], PHE 918[a], LEU 1035[a], LEU 840[a], VAL 914[a], VAL 848[a], ALA 866[a]
Apigetrin	-8.88	311.55 nM	**Conventional Hydrogen Bond** VAL 914[a], LYS 868[a], GLU 885[a]	CYS 1045[a], ILE 915[a], VAL 867[a], GLY 922[a]	**Pi-Sigma** PHE 1047[a] **Pi-Alkyl** CYS 919[a], PHE 918[a], LEU 1035[a], LEU 840[a], VAL 914[a], VAL 848[a], ALA 866[a]
(-)-8-Prenylnaringenin	-10.71	14.04 nM	**Conventional Hydrogen Bond** VAL 914[a], LYS 868[a], ILE 1044[a]	LE 915[a], GLU 885[a], GLU 917[a], VAL 867[a], VAL 898[a], PHE 1047[a], PHE 918[a], LEU 840[a], LEU 1019[a], ASP 1046[a]	**Pi-Cation** LYS 868[a] **Pi-Sigma** LEU 889[a], VAL 916[a], VAL 899[a] **Pi-Alkyl** VAL 848[a], CYS 1045[a], CYS 919[a], ALA 866[a], LEU 1035[a]

Based on the molecular docking results of the VEGFR-2 receptor, the native ligand and cabozantinib as VEGFR-2 inhibitor reference drug demonstrated conventional hydrogen bonding at the amino acid residue ASP 1046[a]. This type of interaction appeared consistently as the primary interaction in 5 out of the 12 compounds tested, which is similar to the hydrogen bonding that occurs in native ligand and reference drug. These findings indicate that conventional hydrogen binding at ASP 1046[a] is a crucial interaction for inhibitory activity towards the VEGFR-2 receptor, which is in consistent with the previous study that identified conventional hydrogen binding at ASP 1046[a] as a determinant of VEGFR-2 inhibitory activity [30]. Among all flavonoid compounds that has conventional hydrogen bond towards ASP 1046[a], hesperetin

emerged as the most promising candidate for VEGFR-2 inhibitor due to its lowest binding energy and inhibition constant value which are -9.57 kcal/mol and 97.00 nM respectively. Furthermore, hesperetin demonstrated the highest similarity toward native ligand and reference drug through 6 similar interactions toward native ligand and 4 with the reference drug, as illustrated in **Fig. 3**.

Table 4. Molecular docking results of *S. littoralis* Hassk. flavonoid compound against c-MET receptor (PDB ID: 3ZZE)

Compound	Binding Energy (kcal/mol)	Inhibition Constant (Ki)	Interactions with Amino Acid Residue		
			Hydrogen bond	Van der Waals	Other bond
Native Ligand	-10.24	31.09 nM	**Conventional Hydrogen Bond** ARG 1208[a], ASN 1209[a], PRO 1158[a], ASP 1222[a]	GLY 1085[a], ALA 1221[a], ILE 1084[a], LEU 1140[a] TYR 1159[a], ASP 1164[a], ASP 1231[a]	**Attractive Charge, Pi-Cation** TYR 1230[a], ASP 1222[a] **Pi-Pi Stacked** TYR 1230[a] **Alkyl, Pi-Alkyl** VAL 1092[a], ALA 1226[a], LYS 1110[a], LEU 1157[a], ALA 1108[a], MET 1211[a], MET 1160[a]
Crizotinib (reference drug)	-9.68	80.25 nM	**Conventional Hydrogen Bond** ALA 1226[a], ASP 1231[a], ASP 1164[a], MET 1160[a] **Carbon Hydrogen Bond** ARG 1208[a]	ASP 1222[a], ALA 1221[a], TYR 1230[a], ASN 1209[a], ARG 1166[a], ASN 1167[a]	**Halogen (Fluorine)** PRO 1158[a]; TYR 1159[a] **Alkyl, Pi-Alkyl** VAL 1092[a], ILE 1084[a], LYS 1110[a], LEU 1140[a], LEU 1157[a], ALA 1108[a], MET 1211[a]
Catechin	-7.41	3700 nM	**Conventional Hydrogen Bond** PRO 1158[a], ARG 1208[a], ASN 1209[a], MET 1160[a]	LEU 1157[a], ALA 1226[a], ASP 1222[a], TYR 1230[a], ILE 1084[a], TYR 1159[a]	**Alkyl, Pi-Alkyl** LEU 1140[a], ALA 1221[a], MET 1211[a], ALA1108[a]
Daidzein	-7.20	5290 nM	**Conventional Hydrogen Bond** ASN 1209[a], PRO 1158[a]	ARG 1208[a], ASP 1164[a], TYR 1159[a], MET 1160[a], ASP 1222[a]	**Pi-Sulfur** MET 1211[a] **Pi-Pi Stacked** TYR 1230[a] **Pi-Alkyl** ALA 1108[a], LEU 1140[a], LEU 1157[a], VAL 1092[a], ALA 1221[a]
Formononetin	-7.56	2890 nM	**Conventional Hydrogen Bond** ASP 1231[a], ASP 1222[a]	ARG 1166[a], ASN 1167[a], LEU 1157[a]	**Amide-Pi Stacked, Pi-Pi Stacked** TYR 1230[a] **Pi-Anion**

			Carbon Hydrogen Bond ASN 1209[a],		ASP 1164[a] **Pi-Sulfur** MET 1211[a] **Alkyl, Pi-Alkyl** ALA 1221[a], LEU 1140[a], ALA 1226[a], ARG 1208[a]
Glycitein	-7.38	3920 nM	**Conventional Hydrogen Bond** PRO 1158[a], ASN 1209[a]	VAL 1092[a], ASP 1164 [a], ARG 1208[a], ASP 1222[a], ALA 1221[a], ALA 1226[a], LEU 1140[a]	**Pi-Pi Stacked** TYR 1230[a] **Alkyl, Pi-Alkyl** ILE 1084[a], ALA 1108[a], MET 1211[a], TYR 1159[a], MET 1160[a], LEU 1157[a]
Luteolin	-7.30	4430 nM	**Conventional Hydrogen Bond** PRO 1158[a], MET 1160[a], ASP 1164[a] **Carbon Hydrogen Bond** GLY 1085[a]	ARG 1086[a], GLY 1163[a], TYR 1159[a], LEU 1157[a], LEU 1140[a]	**Pi-Sigma** ILE 1084[a] **Pi-Pi T-Shaped** TYR 1230[a] **Pi-Alkyl** VAL 1092[a], MET 1211[a] ALA 1108[a] **Unfavorable Donor-Donor** ASN 1167[a]
Apigenin	-7.34	4140 nM	**Conventional Hydrogen Bond** ASN 1209[a], PRO 1158[a]	ASP 1164[a], ASP 1222[a], ARG 1208[a], TYR 1159[a]	**Pi-Pi Stacked, Pi-Pi T-shaped** TYR 1230[a] **Pi-Alkyl** ALA 1221[a], LEU 1157[a], ALA 1108[a], MET 1160[a] LEU 1140[a], MET 1211[a], ALA 1226[a]
Hesperetin	-7.36	4000 nM	**Conventional Hydrogen Bond** TYR 1230[a], ASP 1222[a], ILE 1084[a]	ASP 1231[a], ARG 1086[a], GLY 1085[a], VAL 1092[a], LYS 1110[a], LEU 1157[a]	**Pi-Pi Stacked** TYR 1230[a] **Alkyl, Pi-Alkyl** ALA 1226[a], LEU 1140[a], ALA 1221[a], MET 1211[a]
Naringenin	-7.32	4340 nM	**Conventional Hydrogen Bond** ALA 1226[a], ASP 1222[a], TYR 1230[a], ILE 1084[a]	GLY 1085[a], ASP 1231[a], ARG 1086[a], VAL 1092[a], LEU 1140[a], PHE 1223.a	**Pi-Pi Stacked** TYR 1230[a] **Pi-Alkyl** MET 1211[a], ALA 1221[a] **Unfavorable Donor-Donor** TYR 1230[a]
Kaempferide	-7.54	2960 nM	**Conventional Hydrogen Bond** ASP 1222[a], ALA 1226[a], PRO 1158[a]	TYR 1159[a], ASP 1164[a], ASP 1231[a], ASN 1209[a]	**Pi-Pi Stacked, Pi-Pi T-shaped** TYR 1230[a] **Alkyl, Pi-Alkyl** ARG 1208[a], LEU 1157[a], MET 1160[a],

					LEU 1140[a], ALA 1108[a], ALA 1221[a], MET 1211[a]
Negletein	-7.40	3760 nM	**Conventional Hydrogen Bond** ASP 1222[a], PRO 1158[a]	ASP 1164[a], VAL 1092[a], LEU 1157[a], ALA 1226[a], ASN 1209[a], ARG 1208[a]	**Pi-Pi Stacked** TYR 1230[a] **Alkyl, Pi-Alkyl** ALA 1221[a], MET 1211[a], MET 1160[a], TYR 1159[a], ILE 1084[a], ALA 1108[a], LEU 1140[a]
Apigetrin	-9.43	122.94 nM	**Conventional Hydrogen Bond** ASP 1231[a], MET 1160[a], PRO 1158[a]	ASN 1167[a], ASN 1209[a], ASP 1222[a], LYS 1110[a], LEU 1157[a], ALA 1226[a], LEU 1140[a], ALA 1108[a], TYR 1159[a], ILE 1084[a], VAL 1092[a]	**Pi-Anion** ASP 1164[a] **Pi-Sulfur** MET 1211[a] **Pi-Pi Stacked** TYR 1230[a] **Pi-Alkyl** ALA 1221[a], ARG 1208[a]
(-)-8-Prenylnaringenin	-8.50	585.41 nM	**Conventional Hydrogen Bond** TYR 1230[a], PRO 158[a], MET 1160[a], ARG 1086[a]	ASN 1209[a], ASP 1222[a], LEU 1140[a], TYR 1159[a], ILE 1084[a]	**Pi-Sigma** TYR 1230[a], GLY 1085[a] **Alkyl, Pi-Alkyl** ALA 1221[a], ALA 1226[a], MET 1211[a], ALA 1108[a], LEU 1157[a], VAL 1092[a]

The molecular docking results of the c-MET receptor revealed that crizotinib, as the c-MET inhibitor reference drug, exhibited a conventional hydrogen bond at MET 1160[a], which is a critical interaction that is necessary for the inhibitory activity of c-MET [31]. This specific interaction was seen in four flavonoid compounds, such as catechin, luteolin, apigetrin, and (-)-8-prenylnaringenin. Among the flavonoid compounds that form conventional hydrogen bonds with MET 1160[a], apigetrin was identified as the most potent c-MET inhibitor since it demonstrated the lowest binding energy compared to the other flavonoid compounds, with the value of -9.43 kcal/mol, which was close to crizotinib binding energy (-9.68 kcal/mol).

Despite its larger size, apigetrin binds well to the c-MET receptor. This affinity can be attributed to the glucose moiety, which does not hinder binding but instead contributes additional stabilizing interactions. The attached β-D-glucopyranosyl unit provides extra anchoring points by forming hydrogen bonds with residues such as ASP 1231[a] and PRO 1158[a], thereby compensating for its steric bulk. These additional polar contacts enhance enthalpic stabilization, explaining why apigetrin displays a more favorable binding energy [32,33].

Moreover, apigetrin as presented in Fig 3 also shared 5 similar interactions with the native ligand and reference drug while exhibiting the lowest inhibition constant with the value of 122.94 nM.

Although the flavonoid compounds of bajakah tampala stem (*S. littoralis* Hassk.) demonstrated their potential as VEGFR-2 and c-MET inhibitor, further studies are warranted. Molecular dynamics simulations should be conducted to evaluate hesperetin-VEGFR-2 and apigetrin-c-MET complexes' stability using parameters such as RMSD, RMSF, SASA, hydrogen bonding, and binding free energy calculation to strengthen interaction reliability. Furthermore, comprehensive in vitro and in vivo studies focusing on VEGFR-2 and c-MET are necessary. Lastly, pharmacodynamic evaluations and toxicity assessments are essential to confirm both efficacy and safety before therapeutic application.

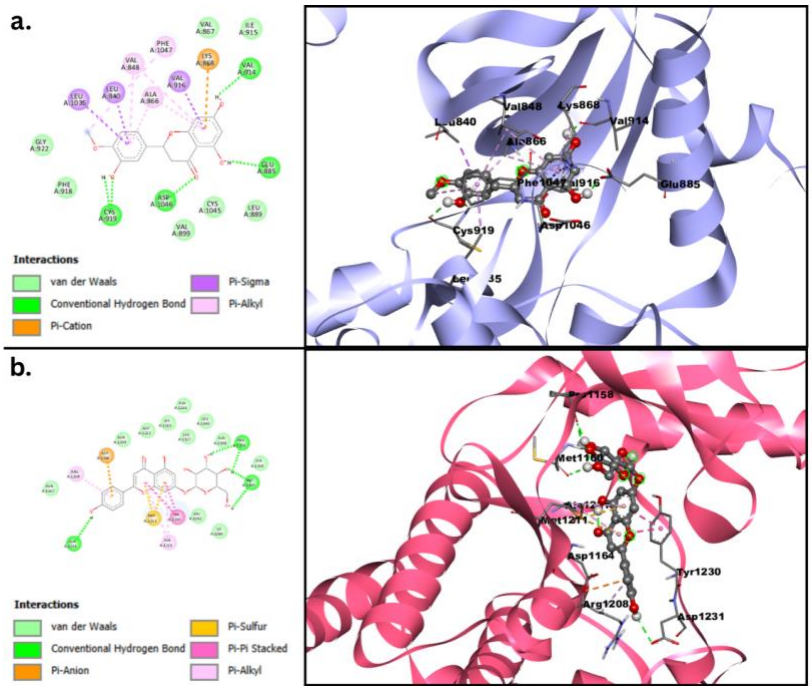

Figure 3. Visualization of 2D and 3D interactions (a) interaction of hesperetin on VEGFR-2 (PDB ID: 2P2I) (b) interaction of apigetrin on c-MET (PDB ID: 3ZZE)

4 Conclusion

In silico analysis of flavonoid compounds from bajakah tampala stem (*S. littoralis* Hassk.) revealed hesperetin and apigetrin as the most favorable predicted binding affinities toward VEGFR-2 and c-MET. Hesperetin has a high affinity for the VEGFR-2 receptor with a binding energy of -9.57 kcal/mol and an inhibition constant of 97.00 nM, while apigetrin exhibited the highest affinity toward c-MET receptor with a binding energy of -9.43 kcal/mol and an inhibition constant value of 122.94 nM. Despite their promising binding affinities, the ADMET predictions revealed notable safety liabilities, including mutagenicity and potential carcinogenicity. These risks highlight the need for further experimental validation before considering any therapeutic development.

References

[1] Dhawale SA., Deokar AV., Firdous MA, Pandit M., Chaudhari MY., Salve SB, et al., 2024, Exploring the potential of small molecules of dual c-Met and VEGFR inhibitors for advances and future drug discovery in cancer therapy, *Future J Pharm Sci.*10: 127.

[2] Bray F., Laversanne M., Sung H., Ferlay J., Siegel RL., Soerjomataram I., et al., 2024, Global cancer statistics 2022: GLOBOCAN estimates of incidence and mortality worldwide for 36 cancers in 185 countries, *CA Cancer J Clin.* 74 (3):229–63.

[3] Lutimba S., Saleem B., Aleem E., Mansour MA., 2024, In Silico Analysis of Triamterene as a Potential Dual Inhibitor of VEGFR-2 and c-Met Receptors, *J Xenobiotics*, 14 (4):1962–87.

[4] Mohamady S., Galal M., Eldehna WM., Gutierrez DC., Ibrahim HS., Elmazar MM., et al., 2020, Dual Targeting of VEGFR2 and C-Met Kinases via the Design and Synthesis of Substituted 3-(Triazolo-thiadiazin-3-yl)indolin-2-one Derivatives as Angiogenesis Inhibitors, *ACS Omega*, 5 (30):18872–86.

[5] Kasai S., Kuwayama N., Motoo Y., Kawashima A., Matsumoto K., Yano S., et al., 2022, Dual blockade of MET and VEGFR2 signaling pathways as a potential therapeutic maneuver for peritoneal carcinomatosis in scirrhous gastric cancer, *Biochem Biophys Res Commun.,* 600:80–6.

[6] Tutunaru CV., Alexandru DO., Dracea SA., Ungureanu L., Popa LG., Beiu C., 2025, Cabozantinib Cutaneous Toxicity—Comprehensive Review, *Life*, 15 (1):72.

[7] Musa S., Amara N., Selawi A., Wang J., Marchini C., Agbarya A., et al., 2024, Overcoming Chemoresistance in Cancer: The Promise of Crizotinib, *Cancers*, 16 (13):2479.

[8] Sianipar RNR., Sutriah K., Iswantini D., Trivadila, Achmadi SS., 2023, Antigout Activity of The Spatholobus littoralis Hassk.

Extract Fractions Against Xanthine Oxidase: Its Metabolite Profile and Inhibition Kinetics, *HAYATI J Biosci*., 31 (1):1–20.

[9] Alhawaris A., 2023, Review: Potency of Borneo Endemic and Typical Plants as Anti-Cancer Medicines, *J Kesehat Pasak Bumi Kalimantan*, 5(1):37.

[10] Iskandar D., Widodo N., Warsito W., Masruri M., Rollando R., Afthoni MH., et al., 2024, Determination of Anticancer from EtOAc Fraction of Spatholobus Littoralis Hassk and of Molecular Structure Prediction, *Maj Obat Tradis*, 29 (2):173.

[11] Sianipar RNR., Suryanegara L., Fatriasari W., Arung ET., Kusuma IW., Achmadi SS., et al., The role of selected flavonoids from bajakah tampala (Spatholobus littoralis Hassk.) stem on cosmetic properties: A review, *Saudi Pharm J*, 31(3):382–400.

[12] Attique SA., Hassan M., Usman M., Atif RM., Mahboob S., Al-Ghanim KA., et al., 2019, A Molecular Docking Approach to Evaluate the Pharmacological Properties of Natural and Synthetic Treatment Candidates for Use against Hypertension, I*nt J Environ Res Public Health*, 16 (6):923.

[13] Vélez LA., Delgado Y., Ferrer-Acosta Y., Suárez-Arroyo IJ., Rodríguez P., Pérez D., 2022, Theoretical Prediction of Gastrointestinal Absorption of Phytochemicals, *Int J Plant Biol*., 13 (2):163–79.

[14] Sreelakshmi V., Raj N., Abraham A., 2017, Evaluation of the Drug-like Properties of Kaempferol, Chrysophanol and Emodin and their Interactions with EGFR Tyrosine Kinase - An *in silico* Approach. *Nat Prod Commun*., 12 (6):915–20.

[15] Jamrozik E., Śmieja M., Podlewska S., 2024, ADMET-PrInt: Evaluation of ADMET Properties: Prediction and Interpretation, *J Chem Inf Model*., 64(5):1425–32.

[16] Rim KT., 2020, In silico prediction of toxicity and its applications for chemicals at work, *Toxicol Environ Health Sci*., 12 (3):191–202.

[17] Rasheed S., Aziz M., Saeed A., Ejaz SA., Channar PA., Zargar S., et al., 2022 Analysis of 1-Aroyl-3-[3-chloro-2-methylphenyl] Thiourea Hybrids as Potent Urease Inhibitors: Synthesis, Biochemical Evaluation and Computational Approach, *Int J Mol Sci*, 23(19):11646.

[18] Zeng F., Wang D., Tian Y., Wang M., Liu R., Xia Z., et al., 2021 Nanoemulsion for Improving the Oral Bioavailability of Hesperetin: Formulation Optimization and Absorption Mechanism, *J Pharm Sci*, 110(6):2555–61.

[19] Morsy HM., Zaky MY., Yassin NYS., Khalifa AYZ., 2025, Nanoparticle-based flavonoid therapeutics: Pioneering biomedical applications in antioxidants, cancer treatment, cardiovascular health, neuroprotection, and cosmeceuticals, *Int J Pharm*, 670:125135.

[20] Halevas EG., Avgoulas DI., Katsipis G., Pantazaki AA., 2022 Flavonoid-liposomes formulations: Physico-chemical characteristics, biological activities and therapeutic applications, *Eur J Med Chem Rep*, 5:100059.

[21] Galkin A., Tammela P., 2023, Natural Product – Drug Interactions and Their Evaluation Using a Caco-2 Cell Culture Model, N*at Prod Commun*, 18 (11): 1–16.

[22] Di L., 2021, An update on the importance of plasma protein binding in drug discovery and development, *Expert Opin Drug Discov*, 16 (12):1453–65.

[23] Seyfinejad B., Ozkan SA., Jouyban A. Recent advances in the determination of unbound concentration and plasma protein binding of drugs: Analytical methods, *Talanta*, 225:122052.

[24] Geldenhuys WJ., Mohammad AS., Adkins CE., Lockman PR., 2015, Molecular Determinants of blood–brain Barrier Permeation, *Ther Deliv*, 6 (8):961–71.

[25] De Lange ECM., Hammarlund Udenaes M., 2022, Understanding the Blood-Brain Barrier and Beyond: Challenges and Opportunities for Novel CNS Therapeutics, *Clin Pharmacol Ther*, 111(4):758–73.

[26] Dias MC., Pinto DCGA., Silva AMS., 2021, Plant Flavonoids: Chemical Characteristics and Biological Activity. *Molecules*. 26 (17):5377.

[27] Sykuła A., Łodyga-Chruścińska E., Garribba E., Kręgiel D., Dzeikala A., Klewicka E., et al., From the Physicochemical Characteristic of Novel Hesperetin Hydrazone to Its In Vitro Antimicrobial Aspects, *Molecules*, 27(3):845.

[28] Ashraf N., Asari A., Yousaf N., Ahmad M., Ahmed M., Faisal A., et al., 2022, Combined 3D-QSAR, molecular docking and dynamics simulations studies to model and design TTK inhibitors, *Front Chem*, 2:10:1003816.

[29] Eid EEM., Azam F., Hassan M., Taban IM., Halim MA., 2018, Zerumbone binding to estrogen receptors: an *in-silico* investigation, *J Recept Signal Transduct*, 38 (4):342–51.

[30] Lv Y., Wang Y., Zheng X., Liang G., 2020, Reveal the interaction mechanism of five old

drugs targeting VEGFR2 through computational simulations, *J Mol Graph Model*, 96:107538.

[31] Damghani T, Sedghamiz T, Sharifi S, Pirhadi S., 2020, Critical c-Met-inhibitor interactions resolved from molecular dynamics simulations of different c-Met complexes, *J Mol Struct*, 1203:127456.

[32] Tabassum T., Kawsar DSMA., 2026, DFT Exploration MEP Molecular Docking and Drug-Likeness as Potent Inhibitors of Monkeypox Viruses of Glucopyranoside Derivatives, *Phys Chem Res*, 14 (1):97–117.

[33] Jamshidi S., Eghbalian A., Shojaei S., Taherkhani A., Feizi-Dehnayebi M., 2025, Flavonoids as Promising Akt1 Inhibitors in Cancer Medicine: Insights From Molecular Docking, Dynamics, DFT Calculations, and In Vitro Validation, *Cancer Rep*, 8 (8):e70315.